ChemComm

Group 13 ion coordination to pyridyl models NAD+ reduction potentials

Journal:	*ChemComm*
Manuscript ID	CC-COM-05-2023-002562.R1
Article Type:	Communication

ARTICLE

Received 00th January 20xx,

Group 13 ion coordination to pyridyl models NAD+ reduction potentials

Leo W. T. Parsons,[a] James C. Fettinger,[a] and Louise A. Berben*[a]

Accepted 00th January 20xx

DOI: 10.1039/x0xx00000x

N-alkylation and N-metallation of pyridine are explored herein to understand how metal-ligand complexes can model NAD+ redox chemistry. Syntheses of substituted dipyrazolylpyridine (pz_2P) compounds $(pz_2P)Me^+$ ($\mathbf{1}^+$) and $(pz_2P)GaCl_2^+$ ($\mathbf{2}^+$) are reported, and compared with $(pz_2P)AlCl_2(THF)^+$ and transition element pz_2P complexes from previous reports. Cyclic voltammetry measurements of cationic $\mathbf{1}^+$ and $\mathbf{2}^+$ show irreversible reduction events ~900 mV anodic those for neutral pz_2P complexes of divalent metals. We proposed that N-metallation using Group 13 ions of 3+ charge provides an electrochemical model for N-alkylated pyridyls like NAD+.

Synthetic pyridyl redox chemistry is inspired by the chemistry of nicotinamide adenine dinucleotide (NAD^+) and nicotinamide adenine dinucleotide phosphate ($NAD(P)^+$) that actively participate in electron transfer (ET) and proton transfer (PT) chemistry in NAD^+[1] and $NAD(P)^+$ dependent enzymes (Chart 1).[2] Pyridyl-based reagents now perform a wide range of redox transformations including hydride transfer,[3] and proton-coupled electron transfer (PCET)[4,5,6] as in reduction of CO_2 by pyridine derivatives with acridine (Acr) and phenanthridine (Phen) (Chart 1).[7] In these hydride transfer reactions two successive ET reactions at pyridinium followed by PT afford dihydropyridinate and large overpotentials are needed to drive ET for catalyst turnover as in CO_2 reduction.[8,9,10]

This work explores the effect of various metal ions on the structure and reduction potential of the pyridine redox site.[11] Tridentate pyridine centred ligands take advantage of the chelate effect to obtain stable metal-pyridyl interactions. We chose a tridentate 2,6-dipyrazolylpyridine (pz_2P) scaffold for this work because the pyridyl central ring has flanking donor groups that are inert to both ET and PT so that chemistry can be localized on the central pyridyl (Chart 1, right).[12,13,14,15] Coordination compounds of pz_2P are reported largely with transition element ions and focus on the metal-centred reaction chemistry.[16,17,18,19] Herein, we compare the redox inert ions Al^{III}, Ga^{III} and Zn^{II} which can promote pyridyl centred redox chemistry as in NAD^+.[20,21] We demonstrate that these redox inert d^0 or d^{10} ions affect pyridyl electronic structure similarly to N-alkylation of pyridyl (Chart 1). Using cyclic voltammetry (CV), we demonstrate that cationic pz_2P complexes of Al^{III} and Ga^{III} provide the best match with the reduction potential for cationic N-methylated pyridyl, with the reduction potential shifted anodically by ~900 mV relative to the neutral pz_2P complexes of Zn^{II},[22] and other divalent transition element ions.[23] This contribution sets the stage for future detailed mechanistic work on the PCET chemistry of NAD^+ models using electrochemical techniques. Prior work has used chemical reagents as redox mediators, which are known promote reactivity additional to the simple ET step; as an example, dithionate reduction byproducts are known modify solution chemistry following ET.[24]

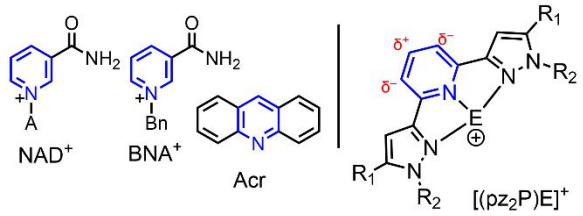

Chart 1. Line drawings: (left) representative pyridyl-based redox mediators. A = Adenine Dinucleotide. (right) of $[(pz_2P)E]^+$. E is a d^0 or d^{10} metal ion (Al^{III}, Ga^{III}) or alkyl.

Synthesis of $\mathbf{1}^+$ and $\mathbf{2}^+$ were achieved starting from isolated pz_2P. *N*-Methylation to form pyridinium or imidazolium salts is often achieved by reaction of pyridine or imidazole with excess methyl iodide (MeI).[25,26] However, reaction of pz_2P with one equivalent methyl iodide in THF yielded no methylated product at room temperature or upon heating to 50 °C over 24 hours. Addition of one equivalent of methyl triflate (MeOTf) to pz_2P in toluene led to precipitation of a white powder identified as $[pz_2(N\text{-}MeP)]OTf$ (**1**-OTf) in 83 % yield based on ^1H and ^{13}C NMR spectra (Scheme 1). *N*-Methylation was evident by observation of a new ^1H resonance at 4.50 ppm which integrated to 3H against the individual pyridyl and pyrazine protons. A single pyrazole proton signal is observed at 6.68 ppm in C_6D_6, indicating a mirror plane of symmetry in the molecule which is

[a] Department of Chemistry, University of California, Davis CA 95616, USA

Electronic Supplementary Information (ESI) available: Synthesis and characterization of compounds, ^1H and ^{13}C NMR, electrochemical data, tables of crystallographic data, crystallographic data (CIF). CCDC 2264174 and 2264175 contains the supplementary crystallographic data for this paper. These data can be obtained free of charge from the Cambridge Crystallographic Data Centre via www.ccdc.cam.ac.uk/data_request/cif. See DOI: 10.1039/x0xx00000x

consistent with selective *N*-methylation of the central pyridine and no methylation of the pyrazole *N*-atoms (Figure S1).

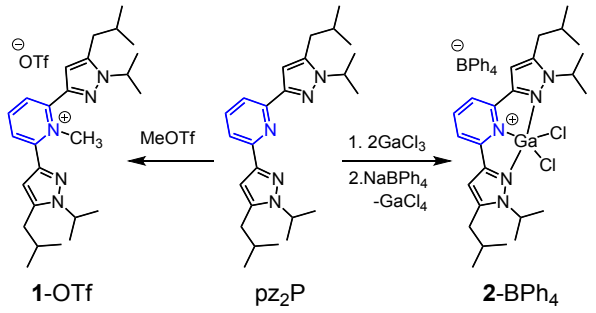

Scheme 1: Synthesis of neutral pz_2P complexes **1**-OTf and **2**-BPh_4.

Synthesis of $[(pz_2P)GaCl_2]GaCl_4$ (**2**-$GaCl_4$) was achieved by addition of two equivalents of $GaCl_3$ dissolved in THF to a solution of pz_2P in THF. After 1 h, the THF was evaporated and the residue was triturated in Et_2O, and **2**-$GaCl_4$ was collected as a white powder in 80% yield (see SI for full synthetic details). The ^1H NMR spectra of **2**-$GaCl_4$ indicates there is no coordinated THF solvate which is different to the prior report of $[(pz_2P)AlCl_2(THF)]AlCl_4$ (**A**-$AlCl_4$) (Figure S2).[27] Single crystals obtained from saturated solutions of **2**-$GaCl_4$ were consistently of poor quality so a metathesis reaction of **2**-$GaCl_4$ with sodium tetraphenylborate ($NaBPh_4$) was performed to isolate $[(pz_2P)GaCl_2]BPh_4$ (**2**-BPh_4) in 69% yield. The proton NMR spectrum of **2**-BPh_4 showed resonances at 7.40, 6.88 and 6.71 ppm integrating to 8H, 8H and 4H, respectively, corresponding to the aryl protons of BPh_4^-. A quartet at 164.55 ppm was observed in the ^{13}C NMR spectra in $CDCl_3$ arising from $^{11}B - ^{13}C$ coupling in BPh_4^- (Figure S3).

Pyridyl ^1H NMR resonances are inequivalent and appear over a wide range, relative to aromatic hydrocarbons such as toluene. The C_o-H, C_m-H, and C_p-H signals appear at 8.53, 6.66, and 6.98 ppm, respectively, for pyridine and the C_o-H/C_p-H and C_m-H signals appear at and 7.02 and 7.13 for toluene in C_6D_6 (atom labelling scheme is shown in Chart 2).[28] As a metric for the polarization of the pyridyl ring by the N heteroatom we focus on the difference in the C_m-H and C_p-H ^1H NMR signals in C_6D_6, denoted as $\Delta\delta(C_m\text{-}C_p)$; smaller differences indicate more even electron shielding as a result of more equal distribution of electron density in the aromatic ring. For pyridine and toluene $\Delta\delta(C_m\text{-}C_p)$ are 0.32 and 0.11, respectively. For substituted pyridines, it is known than electron withdrawing substituents compress $\Delta\delta(C_m\text{-}C_p)$.[29,30]

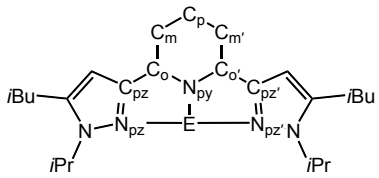

Chart 2. Atom labelling scheme in pz_2P and derivatives used in this work.

For **1**$^+$, **2**$^+$, or **A**$^+$, the C_p-H resonance is observed at 7.61, 8.03, and 7.97 ppm, respectively, which is upfield from 8.27 ppm in pz_2P and is consistent with greater electron density at the C_p atom upon *N*-alkylation or *N*-metalation. The C_m-H resonances in **1**$^+$, **2**$^+$, or **A**$^+$ are at 7.77, 7.84 and 7.52 ppm, respectively, which is a downfield shift from 7.34 ppm in pz_2P. The $\Delta\delta(C_m\text{-}C_p)$ are 0.93, 0.09, 0.20, and 0.19 ppm for pz_2P, **1**$^+$, **2**$^+$, and **A**$^+$, respectively, consistent with the known trend that electron withdrawing substituents such as E^+, on pyridyls compress $\Delta\delta(C_m\text{-}C_p)$. Moreover, the effect of *N*-alkylation or $AlCl_2^+$ or $GaCl_2^+$ coordination on pz_2P are similar. Data reported in C_6D_6 for $(pz_2P)ZnCl_2$ shows that $\Delta\delta(C_m\text{-}C_p)$ = 0.27 ppm (where R_1 = *t*Bu and R_2 = 9-propyl-9-borobicyclo[3.3.1]nonyl, Chart 1), indicating a similar electronic effect of pz_2P coordination to $ZnCl_2$.[22]

Solid-state structures. Crystals of **1**-OTf and **2**-BPh_4 suitable for single crystal X-ray diffraction were obtained from saturated solutions of THF layered with hexanes as colourless blocks and as yellow blocks, respectively (Tables S1, S2, Figure 1). The structure of **1**-OTf shows that the N-pyrazolyl donor atoms are facing in toward the *N*-methyl group and that the methyl group lies out of the plane of the pyridine ring by 9.2°. The structure of **2**-BPh_4 confirms its formulation as a five-coordinate Ga centre. The absence of a THF solvate on the Ga centre in **2**-BPh_4 is in contrast to the structure of **A**-$AlCl_4$ and suggests that the Ga centre is less Lewis acidic than the Al centre in **A**-$AlCl_4$.[27] The coordination geometry about Ga is in between square pyramidal and trigonal bipyramidal, where τ_5 is 0.586.[31] The $N_{pz}\text{-}C_{pz}\text{-}C_{pz'}\text{-}N_{pz'}$ torsion angle is 167.32° for **2**-BPh_4 and is slightly larger than that observed for 6-coordinate **A**-$AlCl_4$ (171.18°). A comparison of pyridyl bond lengths in **1**$^+$, **2**$^+$, **A**-$AlCl_4$ and NAD$^+$ was not insightful due to large errors and variability of the bond length metrics in the structures of published NAD$^+$ structures (Calculation S2, Figure S4).

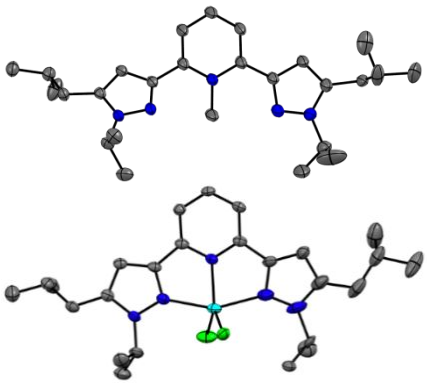

Figure 1: Solid state structures of **1**-OTf (top) and **2**-BPh_4 (bottom). Blue, gray, teal and green ellipsoids represent N, C, Ga, and Cl atoms, respectively. The thermal ellipsoids are shown at 30% probability. Hydrogen atoms and counter ions excluded for clarity.

Electrochemistry Measurements. Cyclic voltammetry (CV) was used to characterize the behaviour of **1**-OTf, **2**-$GaCl_4$, **A**-$AlCl_4$, and pz_2P in 0.3 M Bu_4NBF_4 THF solution, and of **1**-OTf**,** **2**-$GaCl_4$, and pz_2P in 0.1 M Bu_4NBF_4 MeCN solution (Figure 2). **A**-$AlCl_4$ is not stable in MeCN solution.[27] All of the redox features were irreversible. In THF the reduction peak potentials (E_{pc}) for **1**-OTf, **2**-$GaCl_4$, and **A**-$AlCl_4$, are -1.11, -0.98, -1.13 V vs. SCE respectively, and no reduction event was observed within the solvent window for pz_2P in THF. For **A**-$AlCl_4$ the E_{pc} is 150 mV

more cathodic than for $\mathbf{2}^+$ and we attribute this difference to the increased affinity of **A**-$AlCl_4$ for THF as evidenced by the THF solvate in the solid-state structure of **A**-$AlCl_4$. Similarly, the instability of **A**-$AlCl_4$ in MeCN may arise from the greater Lewis acidity of **A**-$AlCl_4$ relative to $\mathbf{2}^+$ which is surprisingly stable in MeCN. In MeCN solution **1**-OTf and **2**-$GaCl_4$, have E_{pc} at -1.20 and -1.03 V vs SCE respectively, and no reduction event was observed within the solvent window for pz_2P.

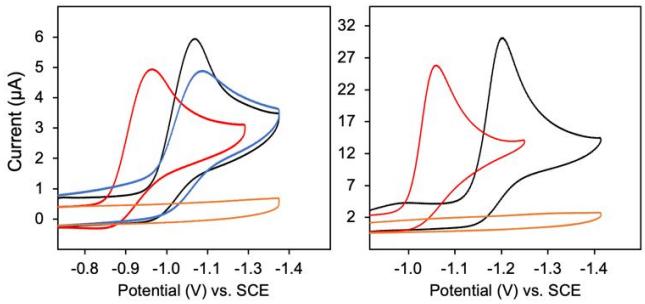

Figure 2. (left) CV's of 0.5 mM **1**-OTf (black), **2**-$GaCl_4$ (red), **A**-$AlCl_4$ (blue), and pz_2P (gold) recorded at 0.1 Vs^{-1} in 0.3 M Bu_4NBF_4 THF. (right) CV's of 0.5 mM **1**-OTf (black) **2**-$GaCl_4$ (red), and pz_2P (gold) recorded at 0.1 Vs^{-1} in 0.1 M Bu_4NBF_4 MeCN.

The E_{pc} values observed here are consistent with reported values for reduction of other *N*-alkylated pyridinium cations,[32,33] and with potentials for ligand-based ET in diiminepyridine (I_2P) Al(III) and Ga(III) complexes.[34,35] This context supports assignment of the irreversible reduction events of **1**-OTf, **2**-$GaCl_4$, and **A**-$AlCl_4$ as pyridine-based. Further, the E_{pc} values in the cationic trivalent Al and Ga ion complexes of pz_2P closely match that for cationic *N*-alkylated **1**-OTf. According to prior reports, ligand based reductive peak potentials are more negative when pz_2P ligands are coordinated to divalent metals in uncharged coordination complexes. As examples, Caulton and coworkers reported a reversible wave with E_{pc} = -2.08 V, and Szymczak and coworkers reported a partially reversible wave at scan rates > 100 mV s^{-1} with E_{pc} = -1.84 V THF, for Fe^{II},[23] and Zn^{II},[22] complexes of pz_2P, respectively. Those E_{pc} values are 700 - 1000 mV more negative than those for **1**-OTf. Complexes of pz_2P with other transition metals display metal-based reductions.[36,37,38]

The similarities in E_{pc} observed between $\mathbf{1}^+$, $\mathbf{2}^+$, $\mathbf{A}^+$, and published NAD^+ mimics likely arise in part from the electrostatic effects of the cationic molecular charge, but not entirely. One study probing the influence of a cation (a proton) in close proximity to a redox site showed an anodic shift in E_{pc} of ~300 mV.[39,40] The remaining ~600 mV anodic shift in E_{pc} observed here may arise from effective interaction between pyridyl-N *p*-orbitals and the valence *p*-orbitals on the alkyl, Al, and Ga ions in $\mathbf{1}^+$, $\mathbf{2}^+$, and $\mathbf{A}^+$; in contrast to transition elements which have *d* valence orbitals. This is consistent with prior work showing metalloaromatic character in Al^{III} and Ga^{III} complexes of I_2P,[41,42] and work where Class III mixed-valency is supported by Al^{III} and Ga^{III} ions that bridge two I_2P ligands.[35,43] Transition element analogs of these two compound classes do not have the same electronic properties.

It is common for synthetic model compounds of NAD^+ to display irreversible CV traces.[44,45,46] This can lead to challenges in determining $E_{1/2}$, although in some cases, at high scan rates (>10,000 Vs^{-1}) and high concentrations (> 1 mM) partial reversibility of the reduction wave for nicotinamide, acridine and quinone organic NAD^+ models can be achieved.[47] We were unable to achieve reversibility with concentrations up to 1 mM and scan rates up to 20 Vs^{-1} using a standard glassy carbon button electrode in MeCN solution (Figure S5). The irreversibility of the CV traces potentially stems from a couple different origins, and these include slow ET kinetics, or a chemical reaction which immediately proceeds the ET event to consume **1**, **2** and **A** which were generated by electrochemical reduction from **1**-OTf, **2**-$GaCl_4$ and **A**-$AlCl_4$, respectively. In experiments designed to probe the irreversibility, changes in E_{pc} with increasing scan rate (υ) were recorded (Figure 3). Plots of current density (j_{pc}) vs. $\upsilon^{0.5}$, for **1**-OTf, **2**-$GaCl_4$ and **A**-$AlCl_4$ in THF, are linear and this indicates a diffusion-controlled process (Figure S6, Calculation S1). We further observed that E_{pc} shifts anodically with increasing υ, and this suggests that an irreversible chemical step likely follows ET on the CV timescale (equations 1 – 3). There are two likely chemical reactions that could follow ET and those are protonation (by trace water) or dimerization:

$$[(pz_2P)E]^+ + e^- \rightarrow (pz_2P)E \qquad \text{eqn 1}$$

$$(pz_2P)E + H^+ \rightarrow (pz_2HP)E \qquad \text{eqn 2}$$

$$(pz_2P)E \rightarrow \tfrac{1}{2}\,[(pz_2P)E]_2 \qquad \text{eqn 3}$$

To determine which of these chemical reactions follows ET we investigated the order of the reaction with respect to **1**-OTf, **2**-$GaCl_4$ and **A**-$AlCl_4$. Since ET is fast, an order dependence of 1 with respect to the analyte will be seen if PT is operative (equation 2), and an order of 2 with respect to the analyte will be observed in the case of dimerization (equation 3). Plots of j_{pc} vs concentration of **1**-OTf and **2**-$GaCl_4$ in the presence of protons show a linear relationship, and support assignment of PT (equation 2) as a possible chemical step following ET as the cause of irreversibility in the CV (Figure S7).

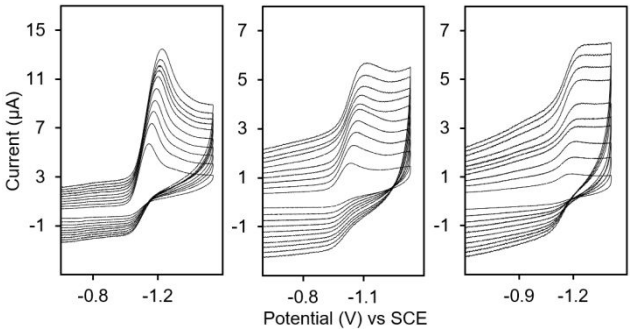

Figure 3. CV's of **1**-OTf (left), **2**-$GaCl_4$ (middle), **A**-$AlCl_4$ (right) in 0.3 M Bu_4NBF_4 THF solution with scan rates 0.1 to 1.0 Vs^{-1}. This data is consistent with a diffusion-controlled process (Figure S5, equation S1) with an irreversible chemical step following ET.

N-methylated and *N*-metalated pyridyl-ligand compounds have been isolated. In each structure the central *N*-functionalized pyridine ring is flanked by pyrazolyl ligands that enhance stability of the compounds. The cationic compounds,

1-OTf, **2**-$GaCl_4$ and **A**-$AlCl_4$, have the form $[(pz_2P)E]^+$ where E = $AlCl_2^+$, $GaCl_2^+$, and CH_3^+, respectively. All three compounds have similar proton NMR resonances and structural features. Irreversible reduction events with E_p between -0.98 and -1.13 V were observed for each of **1**-OTf, **2**-$GaCl_4$ and **A**-$AlCl_4$ in THF solution and demonstrate that cationic pz_2P complexes of trivalent Group 13 cations are good models for E_p of *N*-alkylated pyridine. Our future work will harness these model compounds in understanding PCET mechanisms of NAD^+-inspired dihydropyridinate chemistry.

Conflicts of interest

No conflicts to declare.

Acknowledgements

This manuscript is based on work supported by the National Science Foundation with award CHE-2054529

Notes and references

1 [1] A. Dolega, *Coord. Chem. Rev*., 2010, **254**, 916–937.
2 [2] L. S. Vidal, C. L. Kelly, P. M. Mordaka and J. T. Heap, *Biochim. Biophys. Acta, Proteins Proteomics,* 2018, **1866**, 327−347.
3 [3] E. J. Lawrence, E. R. Clark, L. D. Curless J. M. Courtney, R. J. Blagg, M. J. Ingleson and G. G. Wildgoose, *Chem. Sci.*, 2016, **7**, 2537–2543.
4 [4] P. T. Smith, S. Weng and C. J. Chang, *Inorg. Chem*., 2020, **59**, 9270-9278.
5 [5] C-H. Lim, A. M. Holder, J. T. Hynes and C. B. Musgrave, *J. Am. Chem. Soc.,* 2014, **136**, 16081-16095.
6 [6] A. Marjolin, and J. A. Keith, *ACS Catal*., 2015, **5**, 1123-1130.
7 [7] P. K. Giesbrecht and D. E. Herbert, *ACS Energy Lett*., 2017, **2**, 549-555.
8 [8] S. Ilic, U. P. Kadel, Y. Basdogan, J. A. Keith and K. D. Glusac, *J. Am. Chem. Soc*., 2018, **140**, 4569-4579.
9 [9] S. Ilic, A. Alherz, C. B. Musgrave and K. D. Glusac, *Chem. Soc. Rev.,* 2018, **47**, 2809-2836.
10 [10] S. Ilic, A. Alherz, C. B. Musgrave and K. D. Glusac, *Chem. Commun.,* 2019, **55**, 5583-5586.
11 [11] B. L. Thompson and Z. M. Heiden, *Phys. Chem. Chem. Phys.*, 2021, **23**, 9822-9831.
12 [12] M. A. Halcrow, *Coord. Chem. Rev*., 2005, **249**, 2880-2908.
13 [13] A. V. Polezhaev, C-H. Chen, A. S. Kinne, A. C. Cabelof, R. L. Lord and K. G. Caulton, *Inorg. Chem*., 2017, **56**, 9505-9514.
14 [14] C. Groß, Y. Sun, T. Jost, T. Grimm, M. P. Klein, G. Niedner-Schatteburg, S. Becker and W. R. Thiel, *Chem. Commun.,* 2020, **56**, 368-371.
15 [15] S. Radisavljevic, L. Bratsos, A. Scheurer, J. Korzekwa, R. Masnikosa, A. Tot, N.Gligorijeciv, S. Radulovic and A. R. Simovic, *Dalton Trans.,* 2018, **47**, 13696-13712.
16 [16] P. Weingart, P. Hutchen, A. Damone, M. Kohns, H. Hasse and W. R. Thiel, *ChemCatChem,* 2020, **12**, 3913-3928.
17 [17] Y. Pankratova, D. Aleshin, I. Nikovskiy and Y. Nelyubina, *Inorg. Chem*., 2020, **59**, 7700-7709.
18 [18] N. Suryadevara, A. Mizuno, L. Spieker, S. Salamon, S. Sleziona, A. Maas, E. Pollmann, B. Heinrich, M. Schleberger, H. Wende, A. K. Kuppusamy and M. Ruben, *Chem. Eur. J*., 2022, **28**, e2021035835.
19 [19] J. J. Kiernicki, M. Zeller, and N. K. Szymczak, *Inorg. Chem*., 2020, **59**, 9279-9286.
20 [20] C. D. Cates, T. W. Myers, L. A. Berben, *Inorg. Chem*. 2012, **51**, 11891-11897.
21 [21] T. W. Myers, L. A. Berben, *Chem. Commun*. 2013, **49**, 4175-4177.
22 [22] J. J. Kiernicki, M. Zeller and N. Szymczak, *J. Am. Chem. Soc.,* 2017, **139**, 18194-18197.
23 [23] B. J. Cook, C-H. Chen, M. Pink, R. L. Lord and K. G. Caulton, *Inorg. Chim. Acta*, 2016, **451**, 82-91.
24 [24] M. A. Martini, O. Rudiger, N. Breuer, B. Nöring, S. DeBeer, P. Rodríguez-Maciá and J. A. Birrell, *J. Am. Chem. Soc*., 2021, **143**, 18159–18171.
25 [25] H. Peng, T. Li, D. Tian, H. Yang, G. Xu and W. Tang, *Org. Biomol. Chem*., 2021, **19**, 4237-4337.
26 [26] D. Jo, and S. H. Hong, *Chem. Commun*., 2018, **45**, 487-490.
27 [27] T. J. Sherbow, J. C. Fettinger and L. A. Berben, Inorg. Chem., 2019, 56, 8651-8660.
28 [28] G. R. Fulmer, A. J. M. Miller, N. H. Sherden, H. E. Gottlieb, N. Nudelman, B. M. Stoltz, J. E. Bercaw and K. I. Goldberg, *Organometallics,* 2010, **29**, 2176-2179.
29 [29] A. Gevorgyan, S. Mkrtchyan, T. Grigoryan, V. O. Iaroshenko, *Org. Chem. Front*., 2017, **4**, 2437-2444.
30 [30] J. Liu, K-F. Hu, J-P. Qu, Y-B. Kang, *Org. Lett*., 2017, **19**, 5593-5596.
31 [31] A. W. Addison, T. N. Rao, J. Reedijk, J. van Rijin and G. C. Verschoor, *J. Chem Soc Dalton Trans*., 1984, **7**, 1349-1356.
32 [32] X-Q. Zhu, Y. Tan and C-T. Cao, *J. Phys Chem. B*, 2010, **114**, 2058-2075.
33 [33] H. Zhao, Y. Li and X-Q. Zhu, *ACS Omega*, 2018, **3**, 13598-13608.
34 [34] T. W. Meyers and L. A. Berben, *Inorg. Chem*., 2012, **51**, 1480-1488.
35 [35] A. Arnold, T. J. Sherbow, R. I. Sayler, R. D. Britt, E. J. Thompson, M. T. Munoz, J. C. Fettinger and L. A. Berben, *J. Am. Chem. Soc*., 2019, **141**, 15792-15803.
36 [36] N. S. Labrum, J. Seo, C-H. Chen, M. Pink, D. M. Began and K. G. Caulton, *Inorg. Chem. Acta*, 2019, **486**, 483-491.
37 [37] J. Korzekwa, A. Scheurer, F. W. Heinemann and K. Meyer, *Dalton Trans*., 2017, **46**, 13811-13823.
38 [38] B. J. Cook, M. Pink, K. Pal, and K. G. Caulton, *Inorg. Chem*., 2018, **57**, 6176-6185.
39 [39] N. D. Loewen, S. Pattanayak, R. Herber, J. C. Fettinger, L. A. Berben, *J. Phys. Chem. Lett*., 2021, **12**, 3066-3073.
40 [40] S. Pattanayak, N. D. Loewen, L. A. Berben, *Inorg. Chem*., 2023, **62**, 1919-1925.
41 [41] E. J. Thompson, T. W.Myers, L. A. Berben, *Angew. Chem. Intl. Ed.,* 2014, **53**, 14132-14134.
42 [42] T. M. Bass, C. R. Carr, T. J. Sherbow, J. C. Fettinger, L. A. Berben, *Inorg. Chem*., 2020, **59**, 13517-13523.
43 [43] A. Arnold, T. J. Sherbow, A. M. Bohanon, R. I. Sayler, R. D. Britt, A. L. Smith, J. C. Fettinger, L. A. Berben, *Chem. Sci.*, 2021, **12**, 675-682.
44 [44] J-D. Yang, B-L. Chen and X-Q. Zhu, *J. Phys. Chem. B,* 2018, **122**, 6888-6898.
45 [45] X-Q. Zhu, M-T. Zhang, A. Yu, C-H. Wang and J-P. Cheng, *J. Am. Chem. Soc*., 2008, **130**, 2501-2516.
46 [46] X-Q . Zhu, Y. Tan and C-T. Cao, *J. Phys Chem. B*, 2010, **114**, 2058-2075.
47 [47] A. Anne, P. Hapiot and J.-M. Saveant, *J. Electroanal. Chem.* 1991, **221**, 959-970.

